QUIETDRONES 2024
MANCHESTER
8th - 11th September 2024

Investigation of Ground Effects and Atmospheric Conditions on Noise Perception from Small Aircraft Technologies

Session: Human Response to UAM Noise

Sirine Gharbi, German Aerospace Center (DLR), Innovation Center for Small Aircraft Technologies, Germany, sirine.gharbi@dlr.de
Arthur Schady, German Aerospace Center (DLR), Institute for Atmospheric Physics, Germany, arthur.schady@dlr.de

Abstract: Since urban air mobilities are used for low-altitude operations over populated areas, their realization depends on social acceptance, which is mainly influenced by noise on the ground. Besides psycho-acoustic factors, the perception of noise is affected by ground and atmospheric conditions. Existing aircraft noise prediction models do not consider these effects. Publications have shown that the deviation between simulations and measurements increases with growing lateral distance from the noise source. For an accurate assessment of noise perception from low-flying small aircraft, it is important to include the impact of ground and atmosphere. By applying a particle-based propagation model, these effects are investigated for two different flight altitudes. Simulation results show that downwind the lower-flying airplane is perceived $-4.9\,dB$ quieter, when complex ground and real weather conditions are included. Upwind, a level increase of $+3.6\,dB$ is observed. Weather-dependent optimization of flight paths can contribute to minimizing the perception of noise on communities.
Keywords: Small Aircraft Noise; Ray Acoustics; Meteorology; Ground Effects

1. Introduction

Due to the growing volume of traffic in congested metropolitan cities, the development of concepts for urban air mobility (UAM) is becoming increasingly important. For instance, the fast air transportation of medical goods between clinics and laboratories using small aircraft technologies is in perceptible demand. Simultaneously, the request for express deliveries within nearby cities is rapidly growing. Numerous manufacturers are developing electrically powered, short take-off and landing aircraft (eSTOLs) for flying cabins to facilitate intra-urban and inter-urban passenger and goods transfers (Hildebrandt, A., 2019; Bauranov, A., and Rakas, J., 2021). However, the new vehicle designs, the required infrastructure, and the density of operations pose new challenges for aviation (Vascik, P. D., and Hansman, R. J., 2018; Tojal, M., Hesselink, H., Fransoy, A., and Ventas, E., 2021). The realization of UAM technologies depends, amongst others, on social acceptance, which is primarily influenced by noise immissions on the ground (Ahuja, V., Little, D. S., Majdalani, J., and Hartfield, R. J., 2022). Therefore, in addition to noise reduction at the source, it is necessary to consider sound propagation through the atmosphere and to assess the impact of noise on the population.

Existing semi-empirical aircraft noise prediction models aim to compare different aircraft technologies and designs so that a simplified consideration of the atmosphere and the ground is beneficial for calculating sound propagation. However, several studies by Browne et al. (Browne, R., Munt, R., Simpson, C., and Williams, T., 2004), Munt et al. (Munt, R. M., Browne, R. W., Pidd, M., and Williams, T., 2001) and Parry et al. (Parry, J. A., Van Renterghem, T., Horoshenkov, K. V., and Williams, D. P., 2020) have shown, that for accurate noise prediction on the ground, it is essential to take meteorological gradients into account. Even though advanced aircraft noise prediction models can already distinguish between reflecting ground and absorbing ground, complex ground characteristics are only included with restrictions.

Research by Binder (Binder, U., 2008), Arntzen (Arntzen, M., 2014) and Romond (Romond, R. A., 2021) has dealt with the influence of meteorology and of ground reflections on the sound propagation of large aircraft at high altitudes above $10\,\mathrm{km}$, while the noise caused by low-flying small aircraft close to the ground was not investigated. Rizzi et al. (Rizzi, S., Huff, D., Boyd, D., Bent, P., Henderson, B., Pascioni, K., Sargent, C., and Josephson, D., 2020) summarize the state of the art in the field of UAM noise and emphasize the importance of including atmospheric effects and real ground conditions in sound propagation models to improve noise predictions on the ground which change the public's perception of noise.

Furthermore, previous publications by Römer et al. (Römer, U., Bertsch, L., Mulani, S.B., Schäffer, B., 2022) and Bertsch et al. (Bertsch, L., Schäffer, B., and Guérin, S., 2019) have made the point that the deviations of sound pressure levels between flight tests and aircraft noise models tend to increase with growing lateral distance from the aircraft. The assumption of a simplified atmosphere and surface could be a possible explanation for the discrepancy between noise model results and measurements. Therefore, the primary objective of this work is to provide a better understanding of such uncertainties by establishing a noise-prediction-simulation framework for low-flying small aircraft, which considers inhomogeneous atmospheric conditions and ground effects. This is done by applying the numerical Lagrangian particle-based sound propagation model AKUMET (Heimann, D., 1999). Previously, AKUMET has already been used for static sources in several wind turbine noise applications. In this study, the model is now successively applied to aircraft noise. This work quantifies the noise differences between simplified ground and atmospheric conditions, as used in conventional noise prediction models, relative to real conditions for low-flyover altitudes, and compares the simulation results with noise measurements of flyovers at two different altitudes.

The remainder of this paper is structured as follows. In Section 2 the important influencing factors of outdoor sound propagation are summarized. Section 3 describes the methodological approach by presenting the framework of the simulation for the aircraft noise source. Then, in

section 4, the results are presented and discussed. Finally, in section 5, a conclusion of the work is given.

2. Fundamentals of Outdoor Sound Propagation

In this section, the fundamentals of outdoor sound propagation are introduced. A detailed overview of outdoor sound propagation is given e.g. by Attenborough et al. (Attenborough, K., 2007). Outdoor sound propagation is mainly influenced by atmospheric conditions and ground effects. The formulas that are implemented in AKUMET are presented in the following.

2.1 Acoustic Basics

To consider the volume sensitivity of human hearing, frequency weighting curves are applied to the measured values at different frequencies. Frequency weightings account for the frequency dependence of human sound perception. The low-frequency noise components ($< 100\,Hz$) are not perceived as loud. High-frequency noise components ($> 5000\,Hz$) are perceived as very loud, however, they are appropriately damped by atmospheric absorption and ground reflections. The loudest perceived or most sensitive frequency noise component with the same sound pressure level is around $1000\,Hz$. The most commonly used weighting factors are the so-called A-frequency weighting factors. A detailed description and calculation of the A-rated sound pressure level are provided by Möser et al. (Möser, 2005). At this point, it is expressly mentioned that the perception of noise is individual and can be influenced by the emotional condition of each individual. The presented physical values are measured values and cannot exactly reflect the individual perception of noise.

2.2 Atmospheric Effects on Sound Propagation

Essentially, sound is assumed to propagate in a straight line between the source and the observer. Such a path connects the points of the acoustic wavefront and is referred to as a sound ray. To calculate sound propagation through the inhomogeneous atmosphere, it is fundamental to take into account the physical variables that change in time and space. These include temperature gradients and wind speed gradients, which are responsible for the curvature of acoustic waves (Attenborough, K., 2007). A curved path leads to physical differences in spreading losses, absorption, and ground reflection effects. Curvature due to atmospheric inhomogeneities is called refraction. Using Snell's law, the atmospheric refraction of the sound rays can be calculated. By evaluating the angle of incidence through different layers of the atmosphere, i.e. a discrete region in which the speed of sound c is constant within a layer, the ray path can be determined. The propagation time of the wave results from the summation of the propagation times in the individual layers (Jenssen F. B., Kupermann, W. A., Porter M. B., and Schmidt, H., 2000). The vertical gradient of the speed of sound can be described by various relations. Based on Ruijgrok et al. (Ruijgrok, G.J, 2004) and Pichler et al. (Pichler, H. , 1997) the effective speed of sound c_{eff} is defined as the sum of the temperature-dependent speed of sound part and the part, which depends on the wind vector component in propagation direction with

$$c_{eff}(z) = c_0 + \frac{dT(z)}{dz} \cdot \frac{c_0}{2T_0} \cdot (z + z_g) + w_s \cdot \frac{\log(z/z_0)}{\log(z_r/z_0)} \cdot \cos\beta. \tag{1}$$

where z is the height and starts from the ground, z_g is the level of the ground above sea-level, and $T(z)$ is the vertical temperature profile. The speed of sound at sea-level is given with $c_0 = 340.3\,\mathrm{m/s}$, and $T_0 = 288\,\mathrm{K}$ is the sea-level temperature. For the wind-induced part, w_s describes the wind velocity at a reference height of $z_r = 10\,\mathrm{m}$ and β is the elevation angle between a sound source in the atmosphere to a receiver on the ground. The variable z_0 represents the height at which the horizontal wind speed would disappear according to the logarithmic law. The height z_0 depends on the surface structures of the base and is called the roughness length.

Figure 1 shows exemplary the profile of the speed of sound as a function of altitude, taking into account a negative temperature gradient (green) and a logarithmic wind profile (blue).

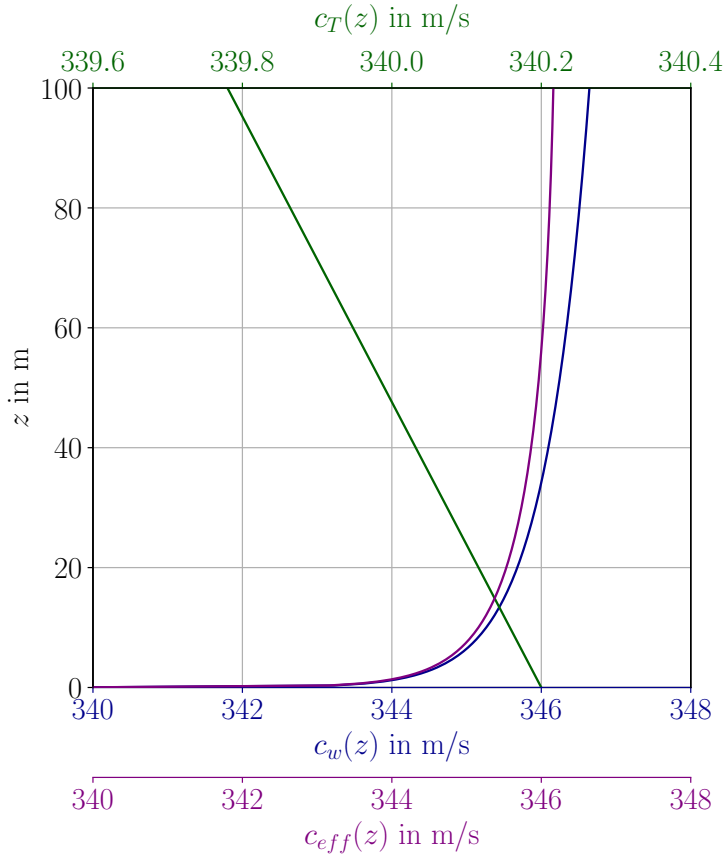

Figure 1: The green line represents the temperature-dependent speed of sound $c_T(z)$, the blue line displays the wind-induced speed of sound $c_w(z)$, and the purple line summarizes the effective speed of sound $c_{eff}(z)$.

If the gradient of the effective speed of sound c_{eff} is positive, i.e. the speed of sound increases with altitude, a ray is curved downwards compared to its straight equivalent. The opposite applies to a negative gradient (Attenborough, K., 2007).

2.3 Ground Effects on Sound Propagation

The influence of the ground on sound propagation depends on the properties of the ground itself and the sound frequency. Once a sound wave hits the ground, it may be reflected or absorbed or subjected to both. Generally, the ground can be characterized as hard ground, porous ground, or mixed ground. Based on the surface type, such as tamped ground or vegetation, the sound is reflected differently (ISO9613-2, 1999). The total sound energy is reflected on the sound-hard ground, while the sound is partially reflected and partially absorbed on the sound-soft ground. In the case of a rough surface, the reflected wave is scattered in different directions, such that the reflection is diffuse. A convenient assumption is that the wave is reflected specularly, i.e. the sound ray is completely reflected in the direction perpendicular to the incident ray. The incident ray and the reflected ray may cause complex interference patterns. Several publications from Attenborough et al. (Attenborough, K., 1985, 1992, 2007) and Salomons (Salomons, E. M., 2001), describe how this effect can be included in the wave equation. The derivation defines a Helmholtz equation for the propagation medium as well as for the ground, including an impedance jump at this boundary. At the boundary, the particle velocity and the sound pressure should be continuous. To calculate the additional attenuation of the sound level due to the influence of the ground, the frequency-dependent reflection coefficient R can be determined by

$$R = \frac{Z_{soil}\cos\theta - Z_{air}}{Z_{soil}\cos\theta + Z_{air}}. \tag{2}$$

In addition to the angle of incidence θ of the sound wave, the specific impedances of the air Z_{air} and the ground Z_{soil} are required to determine R. The impedance of the air Z_{air} is the product of the air density ρ and the speed of sound c. The ground impedance Z_{soil} is different for different ground constitutions, e.g., snow absorbs more sound energy than concrete upon reflection. To determine the impedance of the soil Z_{soil}, Attenborough (Attenborough, K., 1985, 1992) developed various multi-parameter models depending on the flow resistance, the frequency of the incident wave, the porosity of sound-soft soils, and other factors. Since the variables for the application of models that depend on several parameters are often not known, single-parameter models are preferred. Delany and Bazley (Delany, M.E. und Bazley, E.N., 1970) developed an empirical model for calculating the specific impedances of fibrous materials as a function of the frequency f of the sound wave and of the flow resistivity σ, which is the ratio between the applied pressure gradient and the induced volume flow per material thickness, i.e. the difficulty of air to flow through a surface. Typical values of flow resistivity for different soil properties are given by Sutherland et al. (Sutherland, L. C., and Daigle, G. A., 1997). The normalized impedance Z describes the ratio between the specific impedance of the ground Z_{soil} and the sound impedance of the air Z_{air} and can be obtained from the following equation

$$Z = \frac{Z_{soil}}{Z_{air}} = 1 - 9{,}08\left(\frac{f}{\sigma}\right)^{-0.75} + 11.9\,i\left(\frac{f}{\sigma}\right)^{-0.73} \tag{3}$$

Figure 2 illustrates the sound pressure level on the ground for a totally absorbing ground, a totally reflecting ground, and a surface with complex impedance, where the flow resistance of the soil is set to $\sigma = 150\,\mathrm{kPa/m^2 s}$.

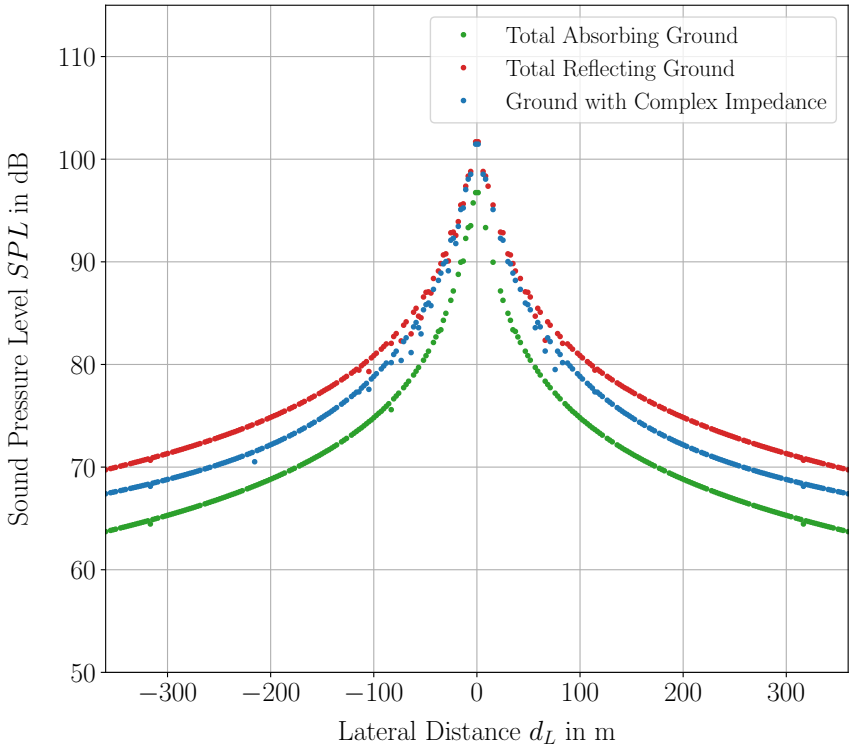

Figure 2: On-ground sound pressure level profiles for different ground conditions for a point source, located at an altitude of $z_{ac} = 30\,ft$, where a homogeneous atmosphere is given with $T_g = 23\,^{\circ}\mathrm{C}$ and $rh = 25\,\%$.

It can be seen that the sound pressure level increases by $6\,\mathrm{dB}$ for a reflecting ground. A surface with complex impedance is somewhere in between. Since the application case presented later is a mowed lawn at the research airfield, a flow resistance of $\sigma = 150\,\mathrm{kPa/m^2 s}$ is assumed for the remainder of this study.

Besides vertical atmospheric gradients and ground effects, the sound level from the source to an observer is also influenced by other atmospheric effects, such as turbulence. For instance, turbulence can cause a dispersion of the sound rays, thus even in shadow zones a sound entry can be present. However, since this paper mainly focuses on ground effects and vertical atmospheric gradients, other effects will not be further discussed.

3. Methodology

To analyze the impact of meteorology and ground conditions on noise perception a sound emission model is combined with a particle-based sound propagation model. Figure 3 shows the methodological approach and the workflow of this study.

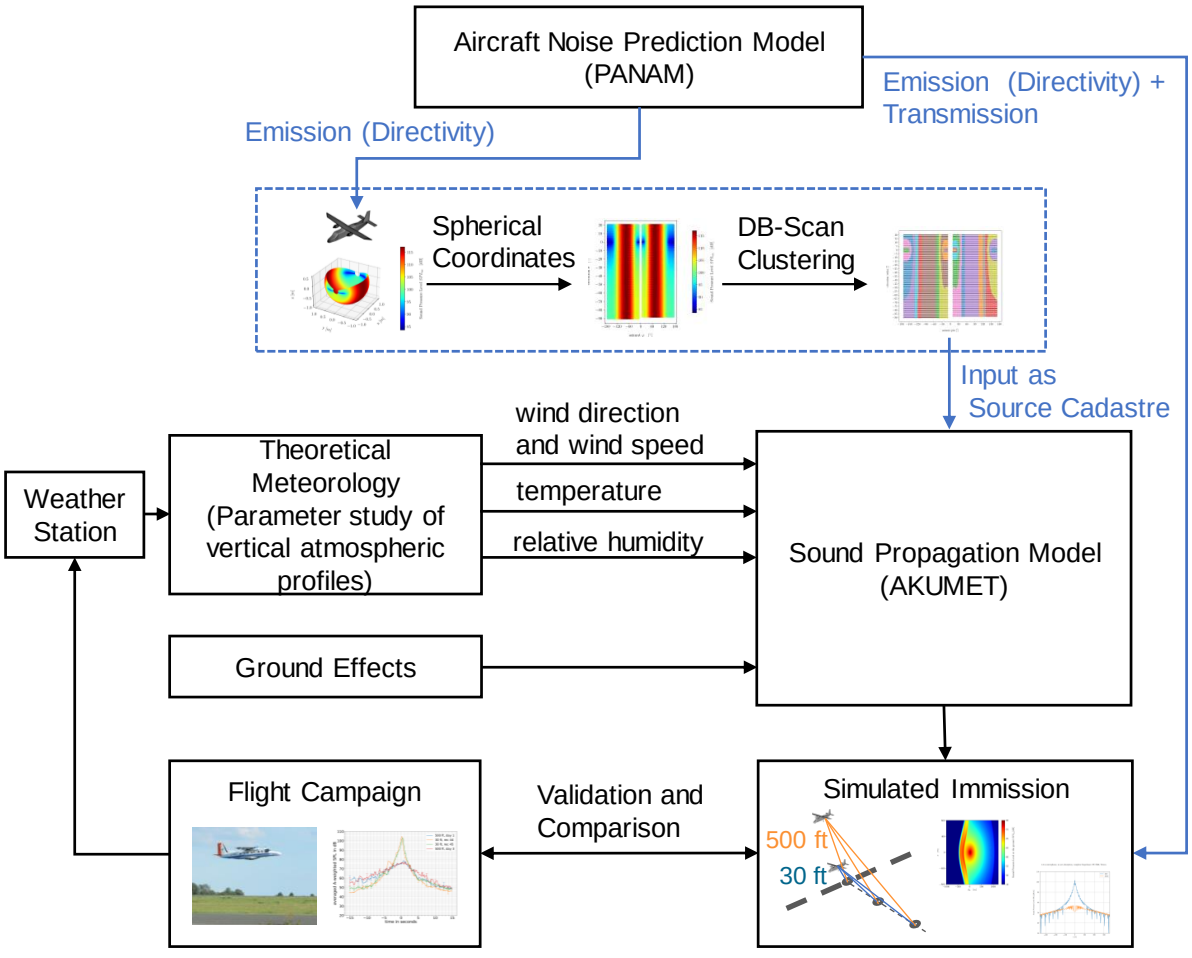

Figure 3: An overview of the tool chain and methodology necessary for a complete aircraft source noise prediction.

The DLR noise prediction model PANAM (Bertsch, L., 2013) is used to calculate the hemisphere of the sound source. When propagating the noise to selected observers, a conventional sound propagation model is applied in PANAM, which cannot take real atmospheric conditions and complex ground impedances into account. Therefore, the calculated emission sphere from PANAM is transferred to the particle-based sound propagation model AKUMET (Heimann, D., 1999). AKUMET

can integrate real atmospheric effects and various complex ground surfaces. Finally, both simulated results of noise immission on the ground are compared with flyover measurements, done by Feldhusen-Hoffmann et al. (Feldhusen-Hoffmann, A., Bertsch, L., Pott-Pollenske, M., Domogalla, V., Kreienfeld, M., and Dörge, N., 2023). In the following, the sound emission model PANAM is presented. Then the numerical sound particle-based model AKUMET is described and the applied case study is shown.

3.1 Sound Emission Model PANAM

In this study, the Parametric Aircraft Noise Analysis Module (PANAM) (Bertsch, L., 2013) is used to simulate the aircraft noise emission at the sound source. Previous work by Bertsch (Bertsch, L., 2013) has shown that the emission model generates valid predictions. PANAM can model each source with directivity and frequency spectrum for each operating condition of the aircraft. According to the aircraft configuration and engine operating condition, the relevant noise sources are accounted for and the sound emission hemisphere at a reference distance of $1\,\mathrm{m}$ is predicted. All individual sources such as the engine, the landing gear, and the aerodynamic geometries of the aircraft are combined and converted to a total source at its center and then exported as a sphere with a radius of $1\,\mathrm{m}$. Noise shielding effects from the aircraft itself can also be taken into account. This results in a frequency spectrum and a directivity of the emitted sound pressure level as output. Besides conventional aircraft with jet engines, small aircraft with propeller propulsion systems are implemented in PANAM. Recently, the analytic propeller noise prediction model from HANSON et al. (Hanson, D. B., and Parzych, D. J, 1993) has been implemented in PANAM (Manghnani, J., Domogalla, V., Ewert, R., Bertsch, L., and Delfs, J., 2024).

To transfer the sound field data at the reference distance, i.e. $1\,\mathrm{m}$, provided by PANAM, to the perceived noise levels at the ground, sound propagation effects have to be considered. To propagate the aircraft noise to the ground, in this study the particle-based model AKUMET is used, as described in the next section 3.2. Taking into account the directivity of the aircraft, the sound propagation model requires a source cadastre where the hemisphere of the aircraft is divided into radiation zones. As shown in Figure 3 the radiation zones are specified as spherical coordinates in azimuth angles φ and elevation angles θ for a radius of $r = 1\,m$. For this purpose, the emission sphere of the aircraft, generated with PANAM, is first transformed into the spherical coordinates φ and θ for AKUMET.

3.2 Sound Propagation Model AKUMET

For long-range sound propagation, ray tracing is advantageous over wave-based methods since ray tracing requires less computational effort. Ray acoustic methods use wavefronts and the presence of rays, which provide a three-dimensional representation of sound propagation and energy flow (Salomons, E. M., 2001).

All simulations in this study are performed with the Lagrangian, particle-based sound propagation model AKUMET (Heimann, D., 1999), developed at DLR. Initially, AKUMET was designed to simulate the propagation of sound over hilly terrain in an inhomogeneous atmosphere for a large domain up to $12\,km$ and can be used for many different applications, e.g. wind turbines or aircraft noise. The applied model showed feasible results as published in Blumrich et al. (Blumrich, R., Coulouvrat, F., and Heimann, D., 2005) and in Heimann et al. (Heimann, D., Käsler, Y., and Gross, G., 2011).

The meteorological field or any vertical profile is taken from the results of a flow model or can be defined manually. AKUMET distributes the emitted sound energy on a given number of sound particles which are then propagated through the atmosphere. Hereby, the paths of the particles describe the propagation of the wavefront. The path of the jth particle is given by the ray vector $\vec{x}_j(t)$ and the unit vector normal to the wavefront $\vec{n}_j(t)$. Differential equations for both vectors are given by

$$\frac{d\vec{x}_j}{dt} = \vec{v_w} + c\vec{n}_j, \tag{4}$$

$$\frac{d\vec{n}_j}{dt} = -\vec{\nabla}c - \sum_{i=1}^{3} n_{ji}\vec{\nabla}v_{wi}, \tag{5}$$

with the speed of sound $c = \sqrt{\kappa RT}$ and $\vec{v_w}$ is the three-dimensional wind vector. Equation 4 and Equation 5 are numerically integrated for all particles using forward time integration until the particle has left the computational domain. The progression of the wavefront $\vec{\tau}(x)$ at two different time steps t_1 and $t_1 + \triangle t$ is given in Figure 4.

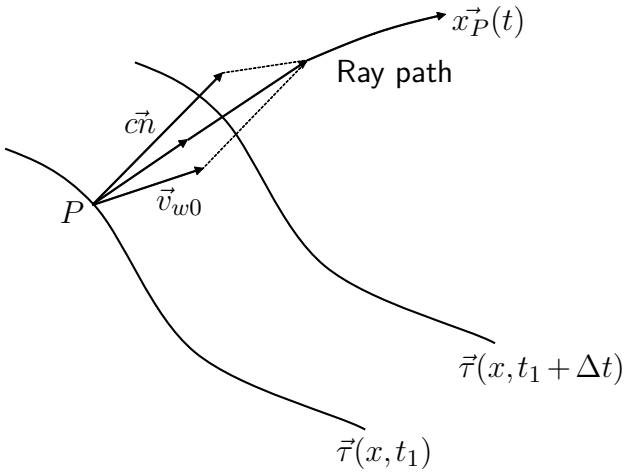

Figure 4: Scheme of ray path determination, where $\vec{\tau}(x)$ represents the wavefront of the sound and $\vec{x_P}(t)$ describes the path of a ray.

At the end of the simulation, the sound pressure level within defined grid cells is computed, based on the number of particles that have passed through that particular grid cell. The model considers the phases of the particles, reflection on the ground, air absorption, refraction, and obstacles of arbitrary shape.

3.3 Application Case

As application case, one to single test-points from a comprehensive measurement flyover campaign with two different flight altitudes have been selected. Details of the measurement setup can be found in Feldhusen-Hoffmann et al. (Feldhusen-Hoffmann, A., Bertsch, L., Pott-Pollenske, M., Domogalla, V., Kreienfeld, M., and Dörge, N., 2023). In these flyover tests, the small airplane Dornier 228 (Do228) overflew microphone stations on the ground. The characteristics of the small airplane Dornier 228 (Do228) are used as a sound source for the simulations and the flyover campaign in this work. The airplane is a two-engine turbine-powered propeller airplane with short take-off and landing capability. The airplane is $15.03\,\mathrm{m}$ long, $4.86\,\mathrm{m}$ high, and has a wingspan of $16.97\,\mathrm{m}$. The maximum take-off weight (MTOW) equates to $5700\,\mathrm{kg}$ and achieves a maximum operating distance of $600\,\mathrm{km}$ at a maximum cruise speed of $370\,\mathrm{km/h}$.

The small airplane is simulated at an altitude of $z_{ac} = 30\,ft$ and $z_{ac} = 500\,ft$ to analyze atmospheric influences and ground effects on sound propagation. Thereby the true airspeed is equal to $56.6\,\mathrm{m/s}$, and the thrust is set to $3.6\,\mathrm{kN}$. An illustration is given in Figure 5. During the flight tests, the aircraft flies over the runway at a constant altitude and the noise is measured by overall 16 microphones located at 6 stations. At positions 1 to 3 in Figure 5, microphones are installed in

$1.2\,\mathrm{m}$ height above the ground, at the sides of the runway redundantly. The microphone at position one is located directly on the runway at $d_L = 0\,\mathrm{m}$. Microphone 2 is situated at $d_L = 70\,\mathrm{m}$ away from the runway, and microphone 3 is positioned at $d_L = 173\,\mathrm{m}$.

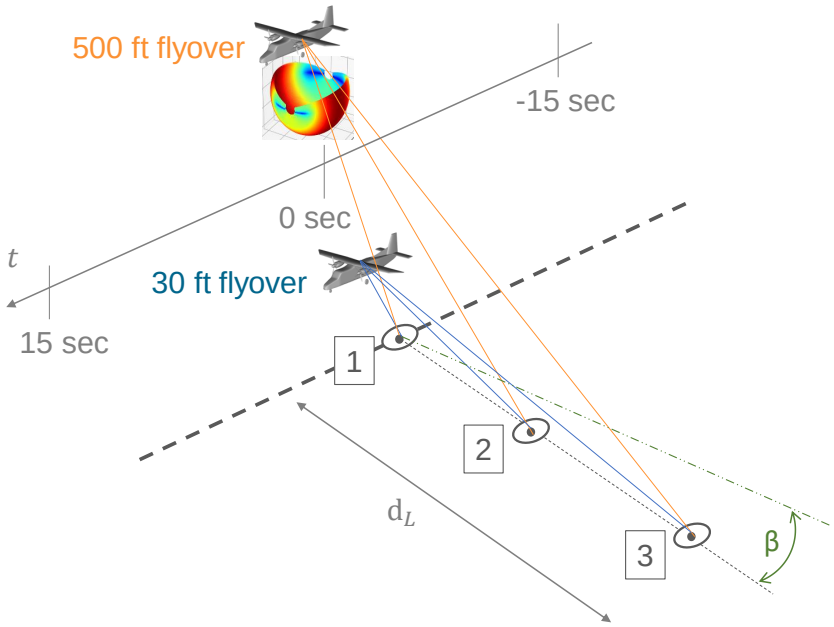

Figure 5: Visualization of the measurement setup together with the sound source characteristics, the directivity of Do288 as the colored sphere.

At the airfield, a weather station is based, which records meteorological data at $2\,\mathrm{m}$ above the ground, such as temperature T_g, total wind velocity vector w_s, wind direction ϕ_w, and the relative humidity rh, during the flight measurements. As shown in Figure 3, using the recorded data, theoretical vertical atmospheric profiles in AKUMET are calculated to determine the sound propagation taking the meteorology into account. The weather conditions for both overflight altitudes are listed in Table 1.

Table 1: Weather conditions at $2\,\mathrm{m}$ above the ground during the flyovers for two altitudes, where T_g describes the temperature and rh is the relative humidity. The wind direction is given with ϕ_w, and the total wind velocity vector is given with w_s, where β indicates the angle to the wind component in the plane from the source to the receptor.

z_{ac} $[ft]$	T_g [°C]	rh [%]	ϕ_w [°]	w_s [m/s]	β [°]
30	23.3	25.3	332.6	2.4	13
500	22.5	30.1	344.1	4.1	2

The dimensions of the acoustical model are chosen as follows: The acoustic grid has 300 cells in the x-direction, 1 cell in the y-direction, and 100 cells in the z-direction with a mesh size of 2.4 m in each dimension. This grid width is chosen to be able to evaluate the sound pressure level at a microphone height of 1.2 m, which corresponds to the center of a cell. The particle number N describes how many particles are emitted and equally distributed in all directions. Thereby the number of particles determines the step width of elevation and azimuth angle and thus the density of particles in the far field away from the source. Particle quantity should be selected small for good computational performance and high for good resolution at receptor volume. For this domain, 5 million particles provide feasible results. Several inhomogeneous atmospheric conditions

are simulated in this work. The temperature decreases linearly with altitude, where the gradient is set to a typical value of $dT/dz = -6.5\,\mathrm{K/km}$. As can be seen from Figure 5 and from Table 1, the small aircraft experiences crosswinds. The angle β specifies the rotational difference between the measured wind direction ϕ_w relative to the wind component in the direction of sound propagation, along d_L. In this work, a logarithmic wind profile is applied, where at $z_r = 10\,m$ above the ground the wind velocity component $w_s \cos\beta$ is set differently, as presented in Table 1. Furthermore, a ground with complex impedance was assumed for the mowed lawn at the airfield, whereby the flow resistance on the ground is simulated with $\sigma = 150\,\mathrm{kPa/m^2 s}$.

In Figure 5 it can be seen, that the Do228 does not radiate homogeneously in all directions. Apart from operating conditions, the directivity depends on airplane geometry, such as the configuration of engines, flaps, and landing gear. For instance, engine noise is the most dominant noise source during take-off, whereas airframe noise predominates during landing (Bertsch, L., 2013). Consequently, for noise exposure on the ground, different spectra, as well as the directivity of an aircraft have to be considered. However, since the primary objective of this work is to analyze the meteorological impact and ground effects on sound propagation, in this study the aircraft is assumed to be a point source. This simplification is made to reduce the complexity and the computation time during the simulation. Since AKUMET requires energy-equivalent levels as input, all individual sound power levels of the directivity are energetically averaged into a total sound power level of $SWL = 122.72\,\mathrm{dB}$. Then, the sound propagation through the atmosphere is calculated.

4. Results

The influence of the surface is first examined and then the interaction with meteorological gradients is investigated. In summary, the simulated results of AKUMET are compared with the output of the conventional aircraft noise prediction model PANAM and are finally validated with the flight measurement results.

Figure 6a illustrates the sound pressure level SPL as a function of the lateral distance d_L to the runway in a homogeneous atmosphere, where the ground has a complex impedance with $\sigma = 150\,\mathrm{kPa/m^2 s}$. For both flight altitudes, it can be seen qualitatively that the sound pressure level decreases with increasing distance due to geometric and atmospheric attenuation. It is particularly notable that at a lateral distance of $d_L = 200\,\mathrm{m}$, the sound pressure level of the two altitudes is equal with $SPL = 72.6\,\mathrm{dB}$. Even further, the sound of the lower-flying airplane is more damped. For instance, at a distance of $d_L = 300\,\mathrm{m}$, the $500\ ft$ high-altitude aircraft is $1.9\,\mathrm{dB}$ louder than for the low-altitude aircraft at $30\ ft$. In the case of a complex ground impedance, this may be due to the different angles of incidence of the sound ray. Multiple reflection as well as refraction effects depend strongly on the angle of incidence.

The deviation of the sound pressure level between both altitudes becomes more significant when the prevailing meteorology is taken into account, see Figure 6b. Considering the prevailing weather conditions, the sound pressure level profile of the aircraft at $500\ ft$ does not differ noticeably, however, the sound pressure level characteristic for the $30\ ft$ high aircraft does change significantly, even if the prevailing wind velocity at $2\,\mathrm{m}$ above the ground for the $500\ ft$ flyover is twice as high, see Table 1. The sound pressure level of the $30\ ft$ flying aircraft is $SPL = 70.5\,\mathrm{dB}$ at a lateral distance of $d_L = 200\,\mathrm{m}$ and is further attenuated to $SPL = 65.5\,\mathrm{dB}$ at $d_L = 300\,\mathrm{m}$. Therefore, the low-flying aircraft is perceived significantly quieter, since at $d_L = 300\,\mathrm{m}$ the deviation to the $500\ ft$ flying aircraft is then $SPL = 4.9\,\mathrm{dB}$ concerning the real weather conditions.

A further observation of the $30\ ft$ low-flying aircraft in Figure 6b is a characteristic increase in sound pressure level at a certain distance in the upwind range (i.e. negative d_L). It can be seen that in the upwind direction, the sound pressure level decreases continuously from $SPL = 101.8\,\mathrm{dB}$ to $SPL = 77.6\,\mathrm{dB}$. At a lateral distance of $d_L = -151\,\mathrm{m}$, the sound pressure level increases again to $SPL = 81.2\,\mathrm{dB}$. The occurrence of this effect is based on interference and refraction phenomena that are simulated in the particle-based model AKUMET. This is caused by increasing energy by

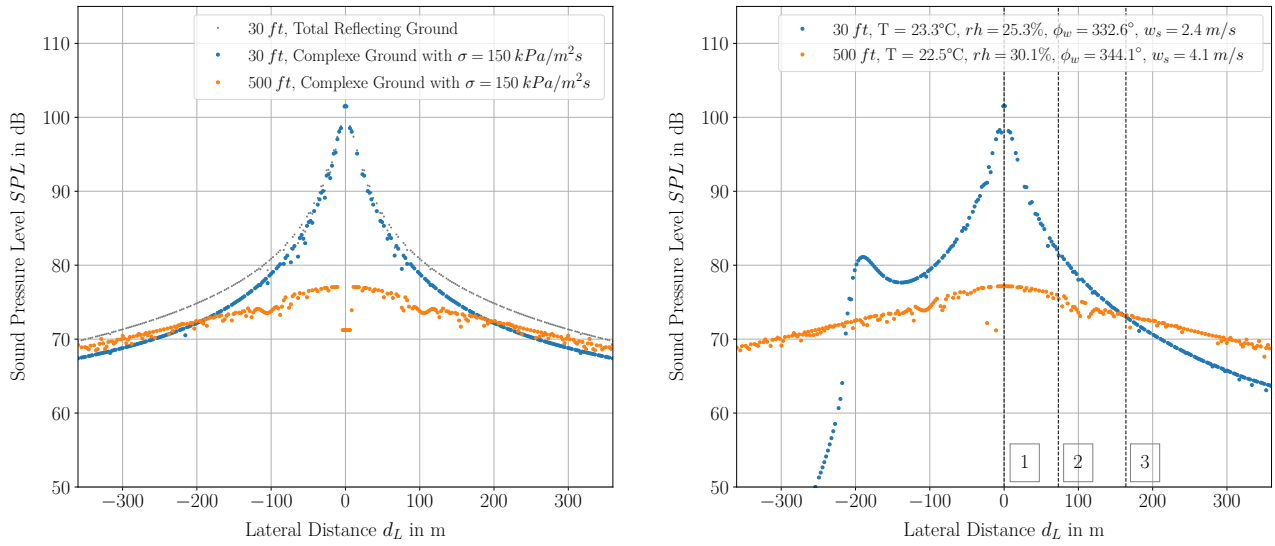

(a) Homogeneous atmosphere.

(b) Real weather prevailing during flight tests.

Figure 6: Sound pressure levels at $1.2\,\mathrm{m}$ above the ground for different altitudes, considering a complex ground with $\sigma = 150\,\mathrm{kPa/m^2\,s}$. The calculations are performed in third-octave bands.

an accumulation of incoherent particles of different frequencies. The upward-refracted rays are crossed with direct incident sound rays. At the crossing point, the sound pressure level increase may occur due to the superposition of sound waves at the crossing point (Elsen, K. M., Bertagnolio, F., and Schady, A., 2023). Depending on the superposition of the sound waves, whether constructive or destructive interference, this can lead to a duplication of pressure amplitude for the noise or even a partial cancellation of the sound. The described effect of the sudden level amplification and extinction is discussed by Elsen et al. (Elsen, K. M., Bertagnolio, F., and Schady, A., 2023), investigating the sound propagation of wind turbines. At this point, it is important to emphasize that this is not a matter of caustics, but of physics that occurs in the superposition of waves, such as reflection on the ground and refraction effects as demonstrated in this work. The particle-based model AKUMET is able to handle such superposition phenomena. This effect only appears for low sound sources and a logarithmic wind profile. Previous aircraft noise propagation models, for instance by Arntzen (Arntzen, M., 2014), do not observe this problem, as on the one hand a linear wind profile is assumed. As a result, there is only an upward curvature of the sound rays in the upwind direction visible, without an intersection of incident and refracted rays. On the other hand, the flight altitude of large aircraft is high enough that the wind gradients near the ground have no influence.

The comparison of the numerical results from the particle-based model AKUMET with the measurement data of the flight campaign (Feldhusen-Hoffmann, A., Bertsch, L., Pott-Pollenske, M., Domogalla, V., Kreienfeld, M., and Dörge, N., 2023) shows a qualitative similar tendency for both altitudes, even if the airplane is assumed to be a monopol in this work. This could be since, as shown in Figure 5, the microphones are aligned at a certain angle to the aircraft. The sound ray of a specific point of the hemisphere hits the ground. At the given angle, the sound ray with the maximum sound pressure level of the emission sphere is propagated. From the measurement results, it can be seen clearly, that the sound, emitted from the $30\ ft$-low-flying aircraft, is attenuated more intensely with increasing lateral distance from the runway. The sound pressure level reduction from microphone 1 to microphone 2 measures $\Delta\, SPL_{1,2} = 20\,\mathrm{dB}$ and the difference from microphone 2 to microphone 3 is $\Delta\, SPL_{2,3} = 8\,\mathrm{dB}$ (Feldhusen-Hoffmann, A., Bertsch, L., Pott-Pollenske, M., Domogalla, V., Kreienfeld, M., and Dörge, N., 2023). This tendency is well reproduced by the numerical particle-based model AKUMET when ground effects and local weather conditions are

taken into account. The discussed phenomena indicate that meteorology has a dominant influence in particular on low-flying noise sources. A closer look at the wind-induced logarithmic speed of sound profile in Figure 1 shows that in the lower layers, the gradients are higher, and therefore the gradients have a stronger influence on sound refraction.

5. Conclusion

Considering the challenges that would arise with the adoption of UAM concepts, noise impact in urban regions is one of them. This paper addresses the problem of aircraft noise emanating from low-flying small aircraft. Existing aircraft noise prediction methods show limitations in including real atmospheric conditions and complex ground properties since their focus is on the comparison of different technologies and certification calculations. However, the presented study shows that various atmospheric conditions and ground effects have a large impact on the propagation and perception of aircraft noise flying at low altitudes, and consequently should not be neglected in aircraft noise prediction models when applied to urban regions. Additionally, the effects of buildings can be taken into account. Multiple reflections or shadowing effects can lead to discontinuous sound pressure level profiles with higher or lower values.

In this work, complex ground and atmospheric effects on sound propagation are investigated with a combination of a noise emission model and a propagation model based on ray acoustics. Subsequently, the computed noise levels on the ground are validated and compared with measured data, where it turns out that the simulated results with AKUMET correspond qualitatively to the measurement results.

The given analysis shows, that if the microphone is positioned laterally far away from the runway, a complex ground impedance has such a considerable influence that the lower flying airplane at $30\,ft$ is perceived quieter than the higher flying aircraft at $500\,ft$. The attenuation of the noise level of the lower flying aircraft even increases when the weather conditions are taken into account. For instance, it is shown that at a distance of $d_L = 300\,m$, the lower-flying aircraft becomes $-4.9\,dB$ quieter. Furthermore, the given investigation demonstrates a characteristic level increase of $+3.6\,dB$ in the upwind direction, which is attributed to refraction interference phenomena and is exclusively observed for low-flying airborne objects and the presence of a logarithmic wind profile. In conclusion, using a homogeneous atmosphere modeling approach will give results that differ from an inhomogeneous atmosphere and hence those methods are error-prone and associated with deviations and uncertainties compared to aircraft noise measurements. The noise prediction uncertainties for a small aircraft operating close to the ground can be in the order of several dB. Since human perception already notices a difference of $3\,dB$, it is of significant importance to consider the sound level deviation due to wind gradients and ground effects. In this paper, a small aircraft is assumed to be the sound source, however, the findings of this study can also be applied to drones and various UAM concepts.

In the present methodology, some limitations have to be recalled. The simulated small aircraft is assumed to be a point source radiating equally in all directions. Since the simulated results provide satisfactory agreement with the measured values, this approximation may be sufficient. Nevertheless, this simplification has to be verified, therefore the directivity will be included in the next study. Apart from that, the occurrence of turbulence in the atmosphere affects sound propagation since turbulence can cause a dispersion of the sound rays, even into shadow zones.

In summary, with increased knowledge of propagation characteristics, engineers are one step toward understanding various noise contours. For instance, the findings from this work can be used to explain deviations and uncertainties between conventional aircraft noise prediction models and real flight tests due to their dependency on weather conditions and soil properties. In addition, certification regulations for potential urban air mobility operations can take into account the knowledge gained about the behavior of the meteorological effects and complex ground characteristics on outdoor sound propagation. Therefore, the present work is one step toward paving the way for

the introduction of UAM on a commercial scale. And possibly one step closer to minimizing the noise impact by determining the quietest flight path, given local weather conditions and ground impedances.

Acknowledgments

This work is part of the DLR project L²INK. The authors are grateful to Lothar Bertsch for providing the emission data of the aircraft, simulated with PANAM, and to Katharina Maria Elsen for instructing AKUMET handling.

References

Ahuja, V., Little, D. S., Majdalani, J., and Hartfield, R. J. (2022). On the prediction of noise generated by urban air mobility (UAM) vehicles. II: Implementation of the Farassat F1A formulation into a modern surface-vorticity panel solver. *Physics of Fluids*, *34*(116118).

Arntzen, M. (2014). *Aircraft noise calculation and synthesis in a non-standard atmosphere* (PhD thesis). Delft University of Technology.

Attenborough, K. (1985). Acoustical impedance models for outdoor ground surfaces. *The Journal of the Acoustical Society of America*, *99*, 521-544.

Attenborough, K. (1992). Ground parameter information for propagation modelling. *The Journal of the Acoustical Society of America*, *92*, 418-427.

Attenborough, K. (2007). Sound Propagation in the Atmospere. *Handbook of Acoustics*.

Bauranov, A., and Rakas, J. (2021). Designing airspace for urban air mobility: A review of concepts and approaches. *Progress in Aerospace Sciences*.

Bertsch, L. (2013). *Noise Prediction within Conceptual Aircraft Design* (PhD thesis). Technische Universitat Braunschweig.

Bertsch, L., Schäffer, B., and Guérin, S. (2019). Uncertainty Analysis for Parametric Aircraft System Noise Prediction. *Journal of Aircraft*.

Binder, U. (2008). *Untersuchung des Einflusses realer atmosphärischer Bedingungen auf die Ausbreitung von Fluglärm (Investigation of the influence of real atmospheric conditions on the propagation of aircraft noise)* (PhD thesis). Freie Universität Berlin.

Blumrich, R., Coulouvrat, F., and Heimann, D. (2005). Variability of focused sonic booms from accelerating supersonic aircraft in consideration of meteorological effects. *The Journal of the Acoustical Society of America*.

Browne, R., Munt, R., Simpson, C., and Williams, T. (2004). Prediction of helicopter noise contours for land use planning. *10th AIAA*.

Delany, M.E. und Bazley, E.N. (1970). Acoustical properties of fibrous absorbent materials. *Applied Acoustics*.

Elsen, K. M., Bertagnolio, F., and Schady, A. (2023). Sound-Propagation-Models in Wind-Energy: A Code2Code-Comparison. *Forum Acusticum*.

Feldhusen-Hoffmann, A., Bertsch, L., Pott-Pollenske, M., Domogalla, V., Kreienfeld, M., and Dörge, N. (2023). Noise and local pollutants of small aircraft: overview of simulation activities and of the first flight test within the DLR project L2INK. *AIAA AVIATION 2023 Forum*.

Hanson, D. B., and Parzych, D. J. (1993). Theory for Noise of Propellers in Angular Inflow with Parametric Studies and Experimental Verification. *Technical Report, Hamilton Standard Division*.

Heimann, D. (1999). Coupled simulation of meteorological parameters and sound level in a narrow valley. *Applied Acoustics*.

Heimann, D., Käsler, Y., and Gross, G. (2011). The wake of a wind turbine and its influence on sound propagation. *Meteorologische Zeitschrift*.

Hildebrandt, A. (2019). CSR und Energiewirtschaft: Mobilität in der dritten Dimension.

ISO9613-2. (1999). *Acoustics: Attenuation of Sound During Propagation Outdoors; Part 2: General Method of Calculation.*

Jenssen F. B., Kupermann, W. A., Porter M. B., and Schmidt, H. (2000). *Computational Ocean Acoustics*. Springer-Verlag.

Manghnani, J., Domogalla, V., Ewert, R., Bertsch, L., and Delfs, J. (2024). A first principle based approach for prediction of tonal noise from isolated and installed propeller. *30th AIAA/CEAS Aeroacoustics Conference*. (Publication in progress)

Möser, M. (2005). *Technische akustik*.

Munt, R. M., Browne, R. W., Pidd, M., and Williams, T. (2001). A measurement and prediction method for determining helicopter noise contours. *27th European Rotorcraft Forum*.

Parry, J. A., Van Renterghem, T., Horoshenkov, K. V., and Williams, D. P. (2020). *Statistical analysis of sound propagation in uncertain, refracting and turbulent atmospheres.*

Pichler, H. . (1997). *Dynamik der Atmosphäre (Dynamics of the atmosphere)*.

Rizzi, S., Huff, D., Boyd, D., Bent, P., Henderson, B., Pascioni, K., Sargent, C., and Josephson, D. (2020). Urban air mobility noise: Current practice, gaps, and recommendations. *Technical Report, NASA*.

Romond, R. A. (2021). *Meteorological reanalysis data inputs for improved aviation noise modeling* (PhD thesis). The Pennsylvania State University.

Ruijgrok, G.J. (2004). Elements of Aviation Acoustics. *Delft University Press*.

Römer, U., Bertsch, L., Mulani, S.B., Schäffer, B. (2022). Uncertainty Quantification for Aircraft Noise Emission Simulation: Methods and Limitations. *AIAA Journal*.

Salomons, E. M. (2001). *Computational Atmospheric Acoustics*. Springer Science.

Sutherland, L. C., and Daigle, G. A. (1997). *Encyclopedia of Acoustics - chapter 32: Atmospheric Sound Propagation*.

Tojal, M., Hesselink, H., Fransoy, A., and Ventas, E. (2021). Analysis of the definition of urban air mobility – how its attributes impact on the development of the concept. *10th International Conference on Air Transport*.

Vascik, P. D., and Hansman, R. J. (2018). Scaling constraints for urban air mobility operations: Air traffic control, ground infrastructure, and noise. *in Proceedings of the 2018 Aviation Technology, Integration, and Operations Conference*.